

## Energy Technology &amp; Environmental Science

High-Selectivity Electrochemical Conversion of CO<sub>2</sub> to Ethanol using a Copper Nanoparticle/N-Doped Graphene ElectrodeYang Song,<sup>[a]</sup> Rui Peng,<sup>[a]</sup> Dale K. Hensley,<sup>[a]</sup> Peter V. Bonnesen,<sup>[a]</sup> Liangbo Liang,<sup>[a]</sup> Zili Wu,<sup>[a, b]</sup> Harry M. Meyer, III,<sup>[c]</sup> Miaofang Chi,<sup>[a]</sup> Cheng Ma,<sup>[a]</sup> Bobby G. Sumpter,<sup>[a, d]</sup> and Adam J. Rondinone<sup>\*[a]</sup>

Though carbon dioxide is a waste product of combustion, it can also be a potential feedstock for the production of fine and commodity organic chemicals provided that an efficient means to convert it to useful organic synthons can be developed. Herein we report a common element, nanostructured catalyst for the direct electrochemical conversion of CO<sub>2</sub> to ethanol with high Faradaic efficiency (63% at -1.2 V vs RHE) and high selectivity (84%) that operates in water and at ambient temper-

ature and pressure. Lacking noble metals or other rare or expensive materials, the catalyst is comprised of Cu nanoparticles on a highly textured, N-doped carbon nanospine film. Electrochemical analysis and density functional theory (DFT) calculations suggest a preliminary mechanism in which active sites on the Cu nanoparticles and the carbon nanospines work in tandem to control the electrochemical reduction of carbon monoxide dimer to alcohol.

## Introduction

Closing the carbon cycle by utilizing CO<sub>2</sub> as a feedstock for currently used commodities, in order to displace a fossil feedstock, is an appropriate intermediate step towards a carbon-free future. Direct electrochemical conversion of CO<sub>2</sub> to useful products has been under investigation for a few decades. Metal-based catalysts, such as copper,<sup>[1]</sup> platinum,<sup>[2]</sup> iron,<sup>[3]</sup> tin,<sup>[4]</sup> silver,<sup>[5]</sup> and gold,<sup>[6]</sup> along with carbons such as g-C<sub>3</sub>N<sub>4</sub><sup>[7]</sup> have been the primary focus for CO<sub>2</sub> reduction, with some very high Faradaic efficiencies for methane conversion. Copper is argu-

ably the best-known metal catalyst for electrochemical CO<sub>2</sub> reduction,<sup>[8]</sup> capable of electrochemically converting CO<sub>2</sub> into more than 30 different products,<sup>[9]</sup> including carbon monoxide (CO), formic acid (HCOOH), methane (CH<sub>4</sub>) and ethylene (C<sub>2</sub>H<sub>4</sub>) or ethane (C<sub>2</sub>H<sub>6</sub>), but efficiency and selectivity for any product heavier than methane are far too low for practical use.<sup>[10]</sup> Competing reactions limit the yield of any one liquid product to single-digit percentages.<sup>[8]</sup>

Polycrystalline Cu foil produces a mixture of compounds in CO<sub>2</sub>-saturated aqueous solutions that are dominated either by H<sub>2</sub> at low overpotential, or by CO and HCOO<sup>-</sup> at high overpotential, or by hydrocarbons and multi-carbon oxygenates at the most extreme potentials.<sup>[9,11]</sup> Theoretical studies predict that graphene-supported Cu nanoparticles would enhance catalytic activity due to the strong Cu-graphene interaction via defect sites,<sup>[12]</sup> which would stabilize the intermediates from CO<sub>2</sub> reduction and improve selectivity towards hydrocarbon products as methane and methanol at lowered overpotential. Early studies revealed that the electrode surface was dominated by adsorbed CO during the CO<sub>2</sub> reduction and that CO acted as intermediate in the production of hydrocarbons.<sup>[13]</sup> Cu produces hydrocarbons and multi-carbon oxygenates when supplied with CO in the absence of CO<sub>2</sub>, but very negative potentials are still required to promote CO reduction over H<sub>2</sub> evolution. Large overpotentials preclude energetically efficient electrolysis and favor hydrocarbons over liquid oxygenates. Recently, high selectivity of CO electroreduction to oxygenates, with ethanol as the major product, was achieved by oxide-derived Cu, in which the surface intermediates were stabilized by the grain boundaries.<sup>[14]</sup>

We previously reported on a highly textured nitrogen-doped, few-layer graphene electrode that presents with a surface of intense folds and spikes, which we termed carbon nano-

[a] Dr. Y. Song, Dr. R. Peng, D. K. Hensley, Dr. P. V. Bonnesen, Dr. L. Liang, Dr. Z. Wu, Dr. M. Chi, Dr. C. Ma, Dr. B. G. Sumpter, Dr. A. J. Rondinone  
Center for Nanophase Materials Sciences  
Oak Ridge National Laboratory  
Oak Ridge TN (USA)  
E-mail: rondinoneaj@ornl.gov

[b] Dr. Z. Wu  
Chemical Sciences Division  
Oak Ridge National Laboratory  
Oak Ridge TN (USA)

[c] Dr. H. M. Meyer, III  
Materials Science and Technology Division  
Oak Ridge National Laboratory  
Oak Ridge TN (USA)

[d] Dr. B. G. Sumpter  
Computer Science and Mathematics Division  
Oak Ridge National Laboratory  
Oak Ridge TN (USA)

Supporting information for this article is available on the WWW under <http://dx.doi.org/10.1002/slct.201601169>

© 2016 The Authors. Published by Wiley-VCH Verlag GmbH & Co. KGaA. This is an open access article under the terms of the Creative Commons Attribution-NonCommercial License, which permits use, distribution and reproduction in any medium, provided the original work is properly cited and is not used for commercial purposes.

spikes or CNS. The CNS structure is disordered due to the high nitrogen content which prevents well-ordered stacking. In the current report, a carbon nanospike (CNS) electrode with electronucleated Cu nanoparticles (Cu/CNS) is shown to have much higher selectivity for CO<sub>2</sub> electroreduction than H<sub>2</sub> evolution, with a subsequent high Faradaic efficiency to produce ethanol. We believe this is achieved both from the high intrinsic CO<sub>2</sub> reduction activity of Cu and from the synergistic interaction between Cu and neighboring CNS, which controls reduction to alcohol. The major CO<sub>2</sub> reduction product is ethanol, which corresponds to a 12 e<sup>-</sup> reduction with H<sub>2</sub>O as the H<sup>+</sup> source,



where  $E^0$  is the equilibrium potential. By comparing Cu/CNS to control electrodes comprised of 1) Cu on glassy carbon and 2) bare CNS, we demonstrate that CO<sub>2</sub> reduction activity is not a simple consequence of either Cu or CNS. While the reaction mechanism is not yet elucidated, we hypothesize an interaction between adjacent catalytic sites on the Cu and CNS, facilitated by the nanostructured morphology of the catalyst that prevents complete electrochemical reduction to ethylene or ethane, resulting in a high yield of ethanol.

## Results and discussion

The bare CNS electrode (Supporting Information Figure S1) was characterized in our previous study as a dense nanotextured carbon film terminated by randomly oriented nanospikes approximately 50–80 nm in length, where each nanospike consists of layers of puckered carbon ending in a ~2 nm wide curled tip.<sup>[15]</sup> The film is grown by a relatively simple direct-current plasma-enhanced chemical vapor deposition reaction using acetylene and ammonia as reagents.

The CNS film grows quickly and adheres well to the highly-doped silicon wafers that were used for this study. Raman spectra indicate that CNS have a similar structure to disordered, few-layer graphene.<sup>[15]</sup> The CNS is not crystalline and does not diffract. XPS indicates a nitrogen doping density of  $5.1 \pm 0.2\%$  atomic, with proportions of pyridinic, pyrrolic (or piperidinic) and graphitic nitrogens of 26, 25 and 37% respectively, with the balance being oxidized N. In the current experiment, nanoparticles of Cu were electronucleated from CuSO<sub>4</sub> solution directly onto the CNS (Supporting Information, Experimental Methods), and imaged via SEM shown in Figure 1. Electronucleation does not require templating surfactants to control the nanoparticle growth, and leaves the particle surfaces clean. The texture of the CNS promotes nucleation resulting in a large number of smaller particles, in comparison to the glassy carbon control which produced larger particles under identical conditions (Supporting Information Figure S2), with a similar amount of Cu deposited. These well-dispersed Cu particles ranged from about 30 nm to 100 nm with average size of 39.18 nm, with a density *ca.*  $2.21 \times 10^9$  particles cm<sup>-2</sup> (Figure 1B inset). According to the average particle size, the coverage of Cu on CNS is *ca.* 14.2%. TEM measurements (Figure 2 inset) confirm particle size observed via SEM. High-resolution

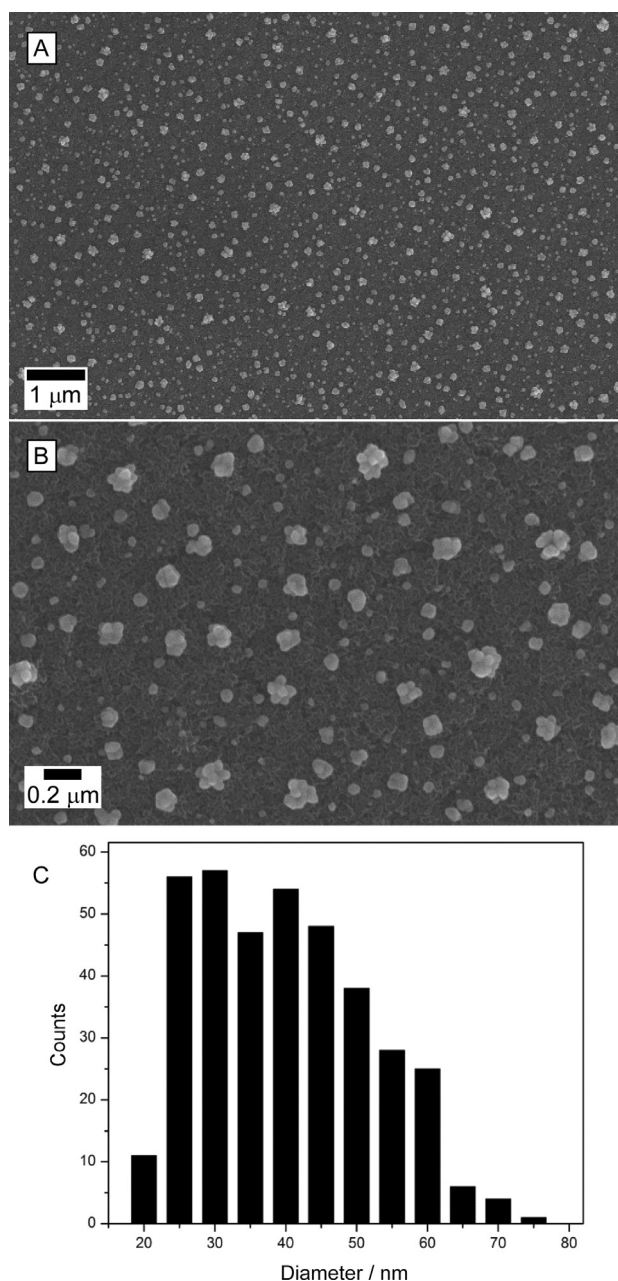


**Figure 1.** Representative SEM images of Cu/CNS electrode with (A) low and (B) high magnification. The average particle size is approximately 39 nm as measured by automated particle sizing of the micrographs.

transmission electron microscopy on scraped samples (HR-TEM) shows the Cu/CNS interface (Figure 2 main) and illustrate a close proximity between Cu and CNS. The lattice spacing of this representative Cu nanoparticle was measured as 0.204 nm, which is consistent with Cu (111). Cu<sub>2</sub>O with lattice spacing *ca.* 0.235 nm were present on the Cu nanoparticles surface in this image, however due to the negative potential applied for Cu deposition, the oxide likely results from exposure to air during sample preparation and transportation between measurements.<sup>[16]</sup> The surface area of the textured surface of CNS and the glassy carbon was measured based on the double layer ca-

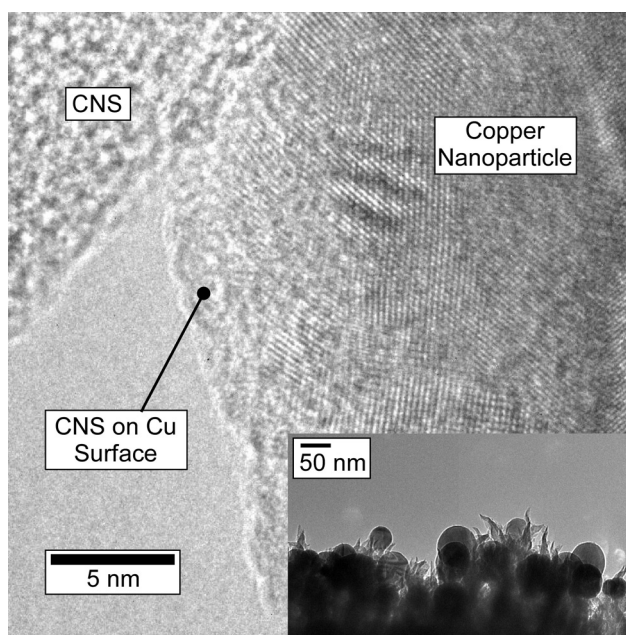


**Figure 2.** HR-TEM of electrodeposited copper nanoparticles on carbon nanospike electrode. Electrodeposited particles are imbedded in N-doped carbon nanospikes providing intimate contact between copper surface and reactive sites in the carbon.

capacitance on both electrodes in 0.1 M KOH. Capacitance was measured by recording anodic-cathodic charging currents (in the potential region where Faradaic processes are absent; see Supporting Information Figure S3). The active surface area of CuNPs was additionally measured by Pb underpotential deposition (Supporting Information) of a representative sample, but could not be measured for each sample without contamination. The Cu nanoparticles typically contribute approximately 8% to the total electrode ECSA for the CNS. To measure the physical stability of the catalyst, SEM images were collected of the particles and the CNS cross sections before and after a 6-hour reduction experiment (Supporting Information Figures S4, S5).

CO<sub>2</sub> electroreduction activity was first measured by linear sweep voltammetry (LSV) in the potential range of  $-0.00$  to  $-1.30$  V vs. RHE at a sweep rate of  $0.05$  V s<sup>-1</sup> as shown in Figure 3. In the presence of CO<sub>2</sub>-saturated potassium bicarbonate electrolyte, using the Cu/CNS, significant anodic shifts in the onset potential are observed compared to that under an argon atmosphere; the onset of activity in CO<sub>2</sub> saturated electrolyte is  $\sim 0.3$  V more positive than in argon purged electrolyte. Note that unlike the featureless voltammograms obtained under an argon atmosphere, a subtle current plateau is obtained at  $\sim -0.9$  V on electrodes with Cu nanoparticle in CO<sub>2</sub> saturated electrolyte. But in the case of pristine CNS electrode, no activity towards CO<sub>2</sub> reduction is observed except the onset of hydrogen evolution at much more negative potential. Larger current densities were obtained in Cu/CNS than either of the controls.

Chronoamperometry (CA) measurements were conducted over a potential range from  $-0.7$  to  $-1.3$  V, which included

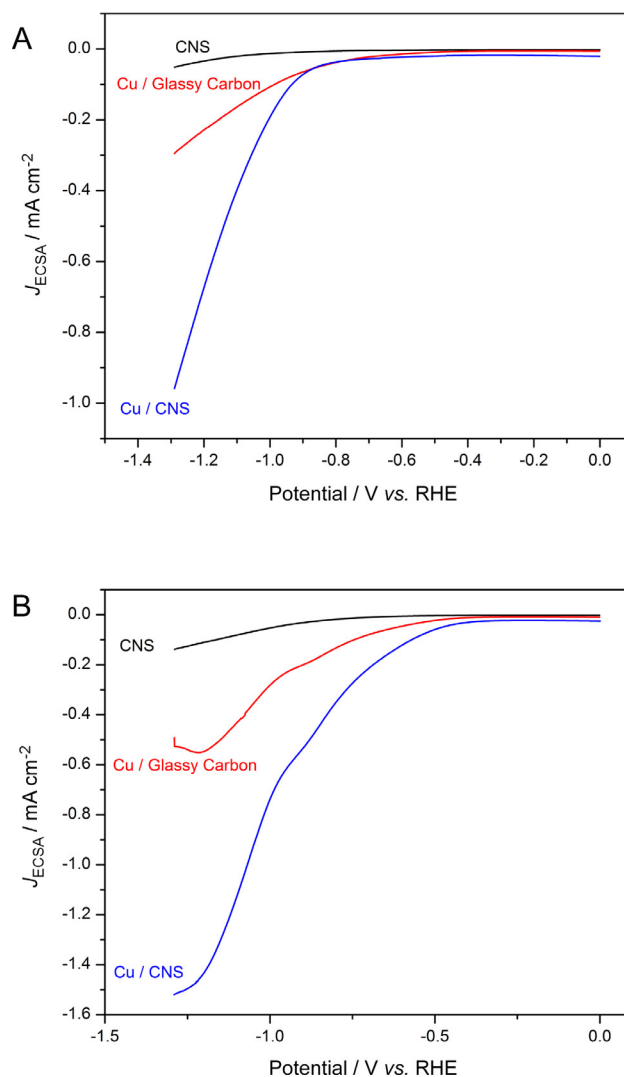


**Figure 3.** LSV curves in potential range of  $0.00$  to  $-1.30$  V vs. RHE at a sweep rate of  $0.05$  V s<sup>-1</sup> in  $0.1$  M KHCO<sub>3</sub> under (A) argon and (B) CO<sub>2</sub> atmosphere on pristine CNS (black), Cu/glassy carbon (red) and Cu/CNS (blue) electrodes. The current density is calculated using the electrochemical surface area (ECSA) of the electrode based on the double layer capacitance on CNS and glassy carbon electrodes in  $0.1$  M KOH, respectively.

these two reduction waves (representative data in Figure 4B for Cu/CNS and Supporting Information Figure S6 A for bare CNS and Cu/glassy carbon controls). New electrodes were fabricated for each data point. The gaseous and liquid products of each CA run were analyzed by gas chromatography (GC) and NMR (of headspace and electrolyte, respectively) to calculate overall current density and Faradaic efficiency for CO<sub>2</sub> reduction and for each product. The overall sustained current density for CO<sub>2</sub> reduction,  $J_{\text{CO}_2 \text{ redn}}$ , increased with more negative potential (Supporting Information Figure S6B) for all three electrodes, consistent with that shown in LSV curves. The Cu/CNS electrode had a greater propensity for CO<sub>2</sub> reduction than either the Cu/glassy carbon or bare CNS electrodes; for instance,  $J_{\text{CO}_2 \text{ redn}}$  from Cu/CNS was 5-fold higher than for bare CNS and 3-fold higher than for Cu/glassy carbon, at  $-1.2$  V.

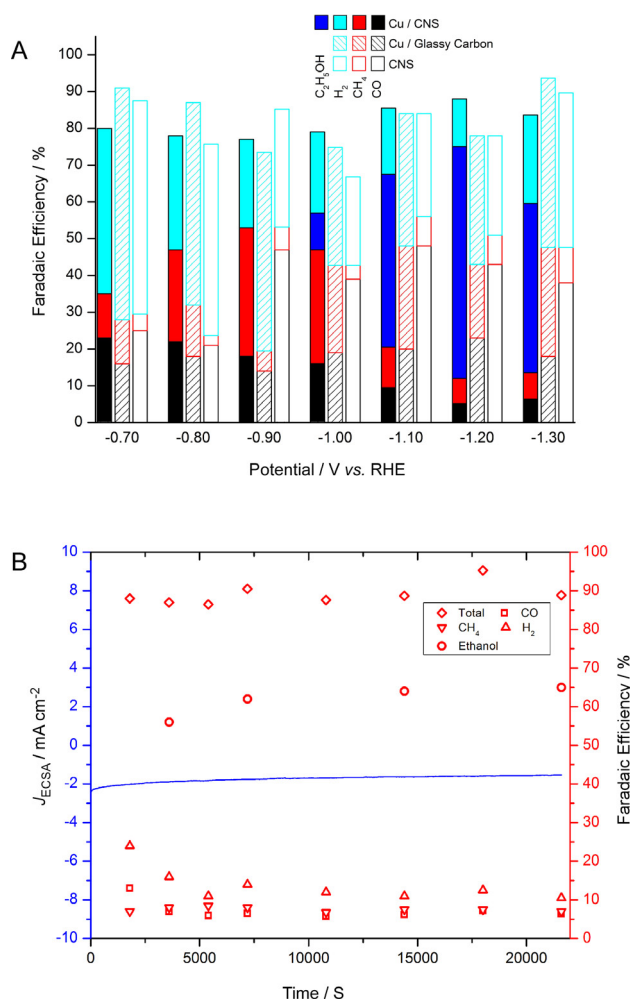


**Figure 4.** Fractional Faradaic efficiency of electrochemical reduction products at various potentials (A). The distribution of products indicates that up to  $-0.9$  V, only gas phase products are produced. At more negative potentials, the rate of CO production on the copper surface is high enough to allow CO dimerization to occur, producing C2 products and subsequently ethanol. Chronoamperometry on Cu/CNS at  $-1.2$  V (B) indicates that the electrode is stable although the distribution of products does change with time, beginning with a higher rate of  $\text{H}_2$  production which drops after the first 5000 seconds. Additional information including relative errors is available in Supporting Information Figure S7.

The fractional Faradaic efficiency was computed by dividing the total electrons into each product (determined independently by chemical analysis) by the total electrons passed during the amperometry experiment. The fractional Faradaic efficiencies for Cu/CNS plus the controls at a range of potentials are shown in Figure 4 A, and for Cu/CNS at  $-1.2$  V over a 6-hour experiment in Figure 4B (Additional data including relative error for Cu/CNS are available in Supporting Information Figure S7). Due to experimental losses between the anode and cathode, the total fractions are less than 100%. The Cu/CNS electrode appears to be stable, as the current density and fractional Faradaic efficiencies for each product barely decreased over the 6 h experiment (Figure 4 A). No significant changes in the Cu nanoparticle size and or CNS thickness was observed

from SEM (Figures S4, S5), indicating that the Cu/CNS is stable under these experimental conditions.

At  $-0.9$  V vs. RHE and more positive potential, only gas phase products  $\text{H}_2$ ,  $\text{CO}$  and  $\text{CH}_4$  were obtained from all three electrodes with  $\text{CH}_4$  as the major product Cu/CNS. In contrast, with bare CNS and Cu/glassy carbon,  $\text{CO}$  was the major product and the  $\text{CO} / \text{CH}_4$  ratio was almost independent of potential. The higher selectivity towards  $\text{CH}_4$  in Cu/CNS indicates a higher degree of surface-bound CO hydrogenation, which is a key step in the formation of  $\text{CH}_4$ .<sup>[17]</sup> At  $-1.0$  V vs. RHE and more negative potential, the current density of  $\text{CO}_2$  reduction increased and ethanol was produced (as a liquid soluble in the aqueous electrolyte) only from Cu/CNS. In comparison, only  $\text{CO}$  and  $\text{CH}_4$  were produced from both control electrodes. At  $-1.3$  V vs. RHE the Cu/glassy carbon also produced trace ethylene (representative GC traces, Supporting Information Figure S8). GC and NMR analysis in search of other products more commonly produced by copper electroreduction, such as methanol or ethane only indicated (representative NMR, Supporting Information Figure S9) occasional trace formate from Cu/CNS.

Examining the breakdown of Faradaic efficiencies for various reactions on Cu/CNS, reveals that at  $-1.2$  V (Figure 4 A), ethanol conversion exhibited the highest efficiency at 63% (that is, 63% of the electrons passing through the electrode were stored as ethanol). Also at  $-1.2$  V vs. RHE, the Faradaic efficiency of gas phase products methane and CO dropped to 6.8% and 5.2%, respectively. The Faradaic efficiency of  $\text{CO}_2$  reduction (competing against water reduction) is 75%. This means that under the best conditions, the overall selectivity of the reduction mechanism for conversion of  $\text{CO}_2$  to ethanol is 84%.

The partial current density and Faradaic efficiency of each product from Cu/CNS electrode at various potentials were illustrated in Figure 5. The partial current density and Faradaic effi-

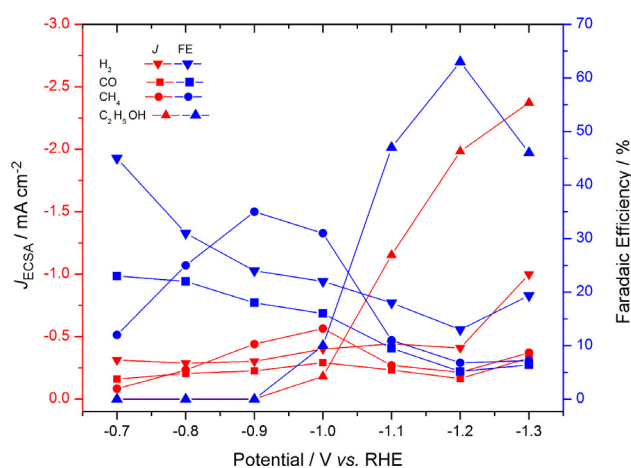


**Figure 5.** Partial current density ( $J$ , red) and Faradaic efficiency (FE, blue) of  $\text{CO}_2$  reduction products from Cu/CNS electrode at various potentials.

ciency for  $\text{CO}$  and methane exhibited a volcanic shape dependence to the potentials applied. The maximum total current

density and Faradaic efficiency were observed at  $-1.0$  V vs. RHE, and decreased when ethanol generation began. The partial current density for ethanol generation increased dramatically with more negative potential until reaching  $-1.2$  V vs. RHE, where the maximum Faradaic efficiency for ethanol generation was also achieved. Above  $-1.2$  V vs. RHE, the rate of increase for ethanol current density was slower, consistent with  $\text{CO}_2$  mass transport limitations. Data were not collected above  $-1.3$  V vs. RHE because hydrogen bubbles that evolved from water reduction blocked the electrode. The decline of Faradaic efficiency for ethanol above  $-1.2$  V vs. RHE suggests that the catalyst reached the mass-transport-limited current density for  $\text{CO}_2$  reduction, and therefore hydrogen evolved via  $\text{H}_2\text{O}$  reduction at unoccupied active sites.

Previous reports of  $\text{CO}_2$  electroreduction on copper have demonstrated a variety of C1 and C2 products, including  $\text{CO}$ ,  $\text{CH}_4$ ,  $\text{CH}_2\text{O}_2$ , ethane, ethylene, ethanol. Heavier hydrocarbons have not been reported as majority products.<sup>[9]</sup> Concerning the reaction mechanism, initial electron transfer to adsorbed  $\text{CO}_2$  will form  $\text{CO}_2^{*-}$  adsr, which can be further reduced to  $\text{CO}_{\text{ads}}$  or other C1 intermediates ( $\text{CHO}_{\text{ads}}$  or  $\text{CH}_2\text{O}_{\text{ads}}$ ) with additional proton-electron transfer.  $\text{CO}$  will result from desorption of  $\text{CO}_{\text{ads}}$  at this stage, or alternatively, further electron transfer to these surface-adsorbed species will lead to  $\text{CH}_4$ .<sup>[1b,13b]</sup>  $\text{CO}_2$  reduction results on the two controls, bare CNS and Cu nanoparticles on glassy carbon, indicate that both Cu metal and CNS are active for electrochemical  $\text{CO}_2$  reduction. On the Cu surface, stronger adsorption of  $\text{CO}$  exists than bare CNS, which provides stable intermediates for further reduction to  $\text{CH}_4$  on Cu/glassy carbon. In contrast,  $\text{CO}$  was released rather than reduced to  $\text{CH}_4$  on bare CNS.

Tafel plots (overpotential vs. the log of partial current density) for  $\text{CO}$  and  $\text{CH}_4$  are shown in Figure 6. For all three samples the plots are linear at low overpotential range with a slope that is consistent with a rate-determining initial electron transfer to  $\text{CO}_2$  to form a surface adsorbed  $\text{CO}_2^{*-}$  intermediate (120 mV / dec), a mechanism that is commonly invoked for metal electrocatalysts.<sup>[8b]</sup> At high overpotential range, steep slopes were obtained, probably indicating control by the combined effects of gas diffusion and ionic mass transport.<sup>[18]</sup> Comparing Cu/CNS to the control electrodes, a direct and intimate contact was introduced between Cu and CNS (Figure 2). Lim et al. predicted a strong interaction between Cu nanoparticles and carbon, and we expect that to extend to CNS as well.<sup>[12]</sup> We expect that the strong interaction provides an environment in which a mechanism involving reactive sites on both the Cu surface and on the N-doped CNS may dominate.

The Cu/CNS catalyst is unusual because it primarily produces ethanol rather than methane or ethylene. Ethanol, as a C2 product, requires carbon-carbon coupling between surface-adsorbed intermediates at some point during the reduction reaction. Recent calculations on C–C coupling on Cu(211) surfaces suggest the kinetic barriers for the coupling are strongly influenced by the degree of the adsorbed  $\text{CO}$  hydrogenation.<sup>[19]</sup> These kinetic barriers tend to decrease with increasing degree of the surface bound  $\text{CO}$  hydrogenation, which can favor the C2 products from  $\text{CO}_2$  reduction.<sup>[20]</sup> A high percentage of C2

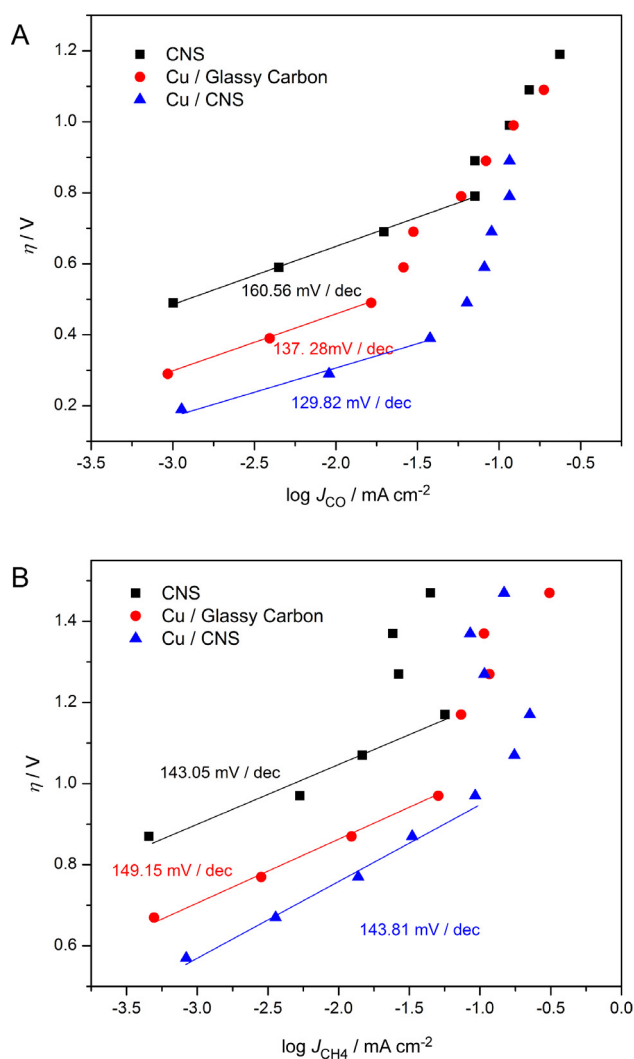


Figure 6. (A)  $\text{CO}$  and (B)  $\text{CH}_4$  partial current density Tafel plots.

products would indicate that coupling is preferred to desorption and loss of C1 intermediates, and this preference for adsorption may be due to the nanostructured nature of the surface. Although initial  $\text{CO}_2$  reduction appears to be the rate-limiting step, the resulting intermediate must be stable enough to persist until a second intermediate is available for C2 coupling. The coupling may be between two surface-bound C1 intermediates, or between a surface-bound C1 intermediate and a nearby C1 intermediate in solution.<sup>[17,21]</sup>

The maximum Faradaic efficiency of ethanol for Cu/CNS is reached at  $-1.2$  V vs. RHE. Further increase in overpotential ( $-1.3$  V vs. RHE) increases  $J_{\text{ethanol}}$  but results in a lower Faradaic efficiency due to an increase in  $\text{H}_2$  production. Hence the proton and electron transfers to C1 become more favorable to produce  $\text{CH}_4$ , which provides a competing pathway against C2 coupling. The details of the reaction mechanism are still to be determined at this time, however there are some lessons in the literature that may yield insights into the high selectivity of this catalyst. Ordinarily, on bulk copper the coupled C2 would continue to be reduced to ethylene or ethane so long as the prod-

uct was in contact with the copper electrode.<sup>[8a,22]</sup> In contrast, with this experiment we have not been able to detect any C2 product except ethanol using the Cu/CNS (ethylene was detected in the control sample Cu/glassy carbon), indicating that the dominant reaction mechanism precludes competitive reduction to ethylene or ethane. Kondo, *et al.* reported that the electronic structure near the Fermi level of graphene is modified in N-doped graphene, where localized  $\pi$  electronic states are reported to form at the neighboring carbon atoms, and propagate anisotropically around the defect due to the perturbation of the  $\pi$ -conjugated system.<sup>[23]</sup> Due to electron-withdrawing effects in the graphene  $\pi$ -conjugated system, the carbon atoms adjacent to nitrogen are positively polarized. This polarization may provide an active site adjacent to the copper for the C2 intermediates to adsorb, which may inhibit complete electroreduction.<sup>[24]</sup> Other doped or defected graphenes are well known to be catalytically active for reactions such as dehydrogenation.<sup>[25]</sup>

First-principles density functional theory (DFT) calculations were carried out to investigate whether the nitrogen dopant or strongly curled morphology in the CNS can help to adsorb the C2 intermediates. As CNS has a similar structure to multilayer graphene, a graphene sheet is adopted to model the interaction between CNS and the C2 intermediates. The dimer of CO, OCCO, was chosen as a C2 intermediate candidate<sup>[19]</sup> for modeling of the interaction with CNS. For a pristine graphene sheet, our calculations suggest the binding energy between OCCO (through one oxygen atom) and graphene is 0.19 eV with a separation distance  $\sim 2.95$  Å (Supporting Information Figure S10 A). For N-doped graphene, the N dopant and adjacent carbon atoms become more active so that the binding energy with OCCO is increased to 0.64 eV with the separation distance shortened to  $\sim 2.70$  Å (Supporting Information Figure S10B). The tripling of the binding energy to 0.64 eV clearly indicates that the C2 intermediates, once formed, can be adsorbed by N-doped CNS fairly strongly and may not desorb easily at room temperature. Furthermore, it is important to note that CNS are puckered and curled, indicating local corrugation on the surface. It has been shown previously that local deformation or buckling could enhance the molecular adsorption on carbon nanotubes and graphene.<sup>[26]</sup> Here we also considered the buckling of pristine and N-doped graphene to investigate the local curvature effect on OCCO adsorption. Upon buckling, the binding energy between OCCO and the concave surface of pristine graphene is increased to 0.34 eV (Supporting Information Figure S10C), while the binding energy between OCCO and the concave surface of N-doped graphene is enhanced to 0.74 eV (Supporting Information Figure S10D). Therefore, the corrugation and curvature naturally embedded into CNS could also help to strengthen the binding between CNS and the C2 intermediates. In addition, we studied the interaction between OCCO and the copper surface, and found that a strong covalent binding is present (when the molecule approaches the Cu surface oriented with one end closer to the surface) with the separation distance reduced to  $\sim 1.98$  Å and binding energy increased to  $\sim 1.21$  eV (Supporting Information Figure S11). Compared to this relatively strong covalent bond,

the binding between OCCO and CNS is weaker, though strong enough to prevent easy desorption of the C2 intermediate. The calculations offer important insights into the observed selective reduction, and we expect that the oxygen atom on one end of the C2 intermediates is covalently bound on reactive copper surface for complete reduction to  $-\text{CH}_3$ , while the oxygen atom on the other end of the C2 intermediates is adsorbed on less reactive CNS and thus protected from complete reduction (hence forming  $-\text{CH}_2\text{OH}$ ), thereby providing a pathway towards selective reduction to ethanol. The possibility that a synergistic effect between Cu and CNS is responsible for the selectivity is surprising given the large size of the Cu nanoparticles, however there is no doubt that the Cu is necessary for this reaction as bare CNS do not produce the same products. Likewise, Cu nanoparticles nucleated on glassy carbon (or any other copper reported to date) do not produce the same products without CNS. While the Cu particles are relatively large, they are on the scale of the CNS which are around 50 nm in length and tend to be imbedded within the spikes. A more detailed understanding of the reaction pathway of such selective reduction of  $\text{CO}_2$  to ethanol warrants further study.

## Conclusion

We report an electrocatalyst which operates at room temperature and in water for the electroreduction of dissolved  $\text{CO}_2$  with high selectivity for ethanol. The overpotential (which might be lowered with the proper electrolyte, and by separating the hydrogen production to another catalyst) probably precludes economic viability for this catalyst, but the high selectivity for a 12-electron reaction suggests that nanostructured surfaces with multiple reactive sites in close proximity can yield novel reaction mechanisms. This suggests that the synergistic effect from interactions between Cu and CNS presents a novel strategy for designing highly selective electrocatalysts. While the entire reaction mechanism has not yet been elucidated, further details would be revealed from conversion of potential intermediates (e.g. CO, formic acid and acetaldehyde) in future work.

## Acknowledgements

This research was conducted at the Center for Nanophase Materials Sciences, which is a Department of Energy (DOE) Office of Science User Facility.

**Keywords:** catalyst · carbon dioxide ·  $\text{CO}_2$  · ethanol · reduction

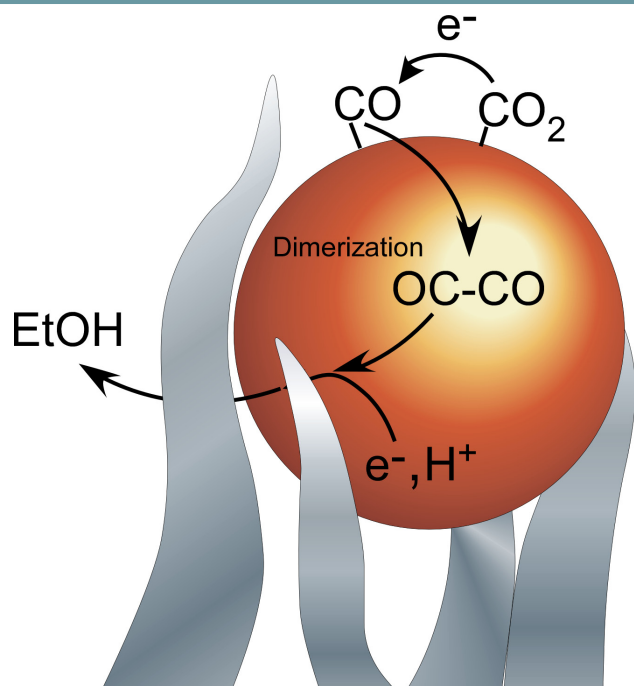
- [1] a) Y. Hori, K. Kikuchi, A. Murata, S. Suzuki, *Chem. Lett.* **1986**, *15*, 897–898; b) Y. Hori, A. Murata, R. Takahashi, *J. Chem. Soc., Faraday Trans. 1* **1989**, *85*, 2309–2326; c) D. W. DeWulf, T. Jin, A. J. Bard, *J. Electrochem. Soc.* **1989**, *136*, 1686–1691.
- [2] a) Y. Tomita, S. Teruya, O. Koga, Y. Hori, *J. Electrochem. Soc.* **2000**, *147*, 4164–4167; b) M. Z. Ertem, S. J. Konezny, C. M. Araujo, V. S. Batista, *J. Phys. Chem. Lett.* **2013**, *4*, 745–748; c) R. Kortlever, I. Peters, S. Koper, M. T. Koper, *ACS Catal.* **2015**.

- [3] a) C. Costentin, S. Drouet, M. Robert, J.-M. Savéant, *Science* **2012**, *338*, 90–94; b) C. Costentin, G. Passard, M. Robert, J.-M. Savéant, *J. Am. Chem. Soc.* **2014**, *136*, 11821–11829.
- [4] Y. Wang, J. Zhou, W. X. Lv, H. L. Fang, W. Wang, *Appl. Surf. Sci.* **2016**, *362*, 394–398.
- [5] a) C. E. Tornow, M. R. Thorson, S. Ma, A. A. Gewirth, P. J. Kenis, *J. Am. Chem. Soc.* **2012**, *134*, 19520–19523; b) J. Rosen, G. S. Hutchings, Q. Lu, S. Rivera, Y. Zhou, D. G. Vlachos, F. Jiao, *ACS Catal.* **2015**, *5*, 4293–4299; c) T. Hatsukade, K. P. Kuhl, E. R. Cave, D. N. Abram, T. F. Jaramillo, *Phys. Chem. Chem. Phys.* **2014**, *16*, 13814–13819.
- [6] a) W. Zhu, Y.-J. Zhang, H. Zhang, H. Lv, Q. Li, R. Michalsky, A. A. Peterson, S. Sun, *J. Am. Chem. Soc.* **2014**, *136*, 16132–16135; b) D. Kim, J. Resasco, Y. Yu, A. M. Asiri, P. Yang, *Nat. Commun.* **2014**, *5*; c) W. Zhu, R. Michalsky, O. n. Metin, H. Lv, S. Guo, C. J. Wright, X. Sun, A. A. Peterson, S. Sun, *J. Am. Chem. Soc.* **2013**, *135*, 16833–16836; d) G. B. Stevens, T. Reda, B. Raguse, *J. Electroanal. Chem.* **2002**, *526*, 125–133.
- [7] S. Ye, R. Wang, M. Z. Wu, Y. P. Yuan, *Appl. Surf. Sci.* **2015**, *358*, 15–27.
- [8] a) Y. Hori, I. Takahashi, O. Koga, N. Hoshi, *J. Phys. Chem. B* **2002**, *106*, 15–17; b) M. Gattrell, N. Gupta, A. Co, *J. Electroanal. Chem.* **2006**, *594*, 1–19.
- [9] K. P. Kuhl, E. R. Cave, D. N. Abram, T. F. Jaramillo, *Energy Environ. Sci.* **2012**, *5*, 7050–7059.
- [10] a) A. M. Appel, J. E. Bercaw, A. B. Bocarsly, H. Dobbek, D. L. DuBois, M. Dupuis, J. G. Ferry, E. Fujita, R. Hille, P. J. Kenis, *Chem. Rev.* **2013**, *113*, 6621–6658; b) S. Ma, P. J. Kenis, *Curr. Opin. Chem. Eng.* **2013**, *2*, 191–199.
- [11] K. Manthiram, B. J. Beberwyck, A. P. Alivisatos, *J. Am. Chem. Soc.* **2014**, *136*, 13319–13325.
- [12] D.-H. Lim, J. H. Jo, D. Y. Shin, J. Wilcox, H. C. Ham, S. W. Nam, *Nanoscale* **2014**, *6*, 5087–5092.
- [13] a) Y. Hori, A. Murata, R. Takahashi, S. Suzuki, *J. Am. Chem. Soc.* **1987**, *109*, 5022–5023; b) J. Kim, D. Summers, K. Frese, *J. Electroanal. Chem. Interf. Electrochem.* **1988**, *245*, 223–244.
- [14] C. W. Li, J. Ciston, M. W. Kanan, *Nature* **2014**, *508*, 504–507.
- [15] L. B. Sheridan, D. K. Hensley, N. V. Lavrik, S. C. Smith, V. Schwartz, C. Liang, Z. Wu, H. M. Meyer, A. J. Rondinone, *J. Electrochem. Soc.* **2014**, *161*, H558–H563.
- [16] M. Pourbaix, *J. Electroanal. Chem.* **1967**, *13*, 471–&.
- [17] A. A. Peterson, F. Abild-Pedersen, F. Studt, J. Rossmeisl, J. K. Nørskov, *Energy Environ. Sci.* **2010**, *3*, 1311–1315.
- [18] M. L. Perry, J. Newman, E. J. Cairns, *J. Electrochem. Soc.* **1998**, *145*, 5–15.
- [19] J. H. Montoya, A. A. Peterson, J. K. Nørskov, *ChemCatChem* **2013**, *5*, 737–742.
- [20] R. Kas, R. Kortlever, A. Milbrat, M. T. M. Koper, G. Mul, J. Baltrusaitis, *Phys. Chem. Chem. Phys.* **2014**, *16*, 12194–12201.
- [21] F. Calle-Vallejo, M. T. M. Koper, *Angew. Chem. Int. Edit.* **2013**, *52*, 7282–7285.
- [22] a) W. Tang, A. A. Peterson, A. S. Varela, Z. P. Jovanov, L. Bech, W. J. Durand, S. Dahl, J. K. Nørskov, I. Chorkendorff, *Phys. Chem. Chem. Phys.* **2012**, *14*, 76–81; b) I. Takahashi, O. Koga, N. Hoshi, Y. Hori, *J. Electroanal. Chem.* **2002**, *533*, 135–143.
- [23] T. Kondo, Y. Honma, J. Oh, T. Machida, J. Nakamura, *Phys. Rev. B* **2010**, *82*, 153414.
- [24] a) K. Gong, F. Du, Z. Xia, M. Durstock, L. Dai, *Science* **2009**, *323*, 760–764; b) L. Zhang, J. Niu, L. Dai, Z. Xia, *Langmuir* **2012**, *28*, 7542–7550; c) L. Zhang, Z. Xia, *J. Phys. Chem. C* **2011**, *115*, 11170–11176.
- [25] a) Z. W. Tang, H. Chen, X. W. Chen, L. M. Wu, X. B. Yu, *J. Am. Chem. Soc.* **2012**, *134*, 5464–5467; b) V. Schwartz, W. J. Fu, Y. T. Tsai, H. M. Meyer, A. J. Rondinone, J. H. Chen, Z. L. Wu, S. H. Overbury, C. D. Liang, *ChemSusChem* **2013**, *6*, 840–846; c) G. K. P. Dathar, Y. T. Tsai, K. Gierszal, Y. Xu, C. D. Liang, A. J. Rondinone, S. H. Overbury, V. Schwartz, *ChemSusChem* **2014**, *7*, 483–491; d) X. J. Cui, Y. H. Li, S. Bachmann, M. Scalone, A. E. Surkus, K. Junge, C. Topf, M. Beller, *J. Am. Chem. Soc.* **2015**, *137*, 10652–10658.
- [26] a) L. B. da Silva, S. B. Fagan, R. Mota, *Nano Lett.* **2004**, *4*, 65–67; b) V. Tozzini, V. Pellegrini, *J. Phys. Chem. C* **2011**, *115*, 25523–25528.

Submitted: August 23, 2016

Accepted: August 30, 2016

## FULL PAPERS



Dr. Y. Song, Dr. R. Peng, D. K. Hensley,  
Dr. P. V. Bonnesen, Dr. L. Liang, Dr. Z.  
Wu, Dr. H. M. Meyer, III, Dr. M. Chi,  
Dr. C. Ma, Dr. B. G. Sumpter, Dr. A. J.  
Rondinone\*

1 – 8

**High-Selectivity Electrochemical  
Conversion of CO<sub>2</sub> to Ethanol  
using a Copper Nanoparticle/N-  
Doped Graphene Electrode**



A nanostructured catalyst achieves one-pot electrochemical conversion of carbon dioxide to ethanol. The catalyst is comprised of copper nanoparticles imbedded in N-doped carbon nanospikes. Carbon dioxide is

electrochemically reduced on copper particles to carbon monoxide, which dimerizes. Electrochemical reduction of the dimer yields ethanol with an overall Faradaic efficiency of 63%.